ELSEVIER

Journal of Nuclear Materials 313–316 (2003) 311–320

journal of nuclear materials

www.elsevier.com/locate/jnucmat

Short and long range transport of materials eroded from wall components in fusion devices

P. Wienhold [a,*], V. Philipps [a], A. Kirschner [a], A. Huber [a], J. von Seggern [a], H.G. Esser [a], D. Hildebrandt [b], M. Mayer [c], M. Rubel [d], W. Schneider [b]

[a] *Institute of Plasma Physics, Research Centre Jülich, Forschungszentrum Jülich GmbH, Ass. EURATOM-KFA, Trilateral Euregio Cluster, P.O. Box 1913, D-52425 Jülich, Germany*

[b] *Max-Planck-Institute of Plasma Physics, Ass. EURATOM, D-10117 Berlin, Germany*

[c] *Max-Planck-Institute of Plasma Physics, Ass. EURATOM, D-85748 Garching, Germany*

[d] *Royal Institute of Technology, Alfvén Laboratory, Ass. EURATOM-VR, S-10044 Stockholm, Sweden*

Abstract

Carbon sources and the sinks have been quantified in TEXTOR and are discussed in terms of short and long range transport. The major source (22 g/h) is the graphite belt limiter, but part (10 g/h) of the carbon is directly re-deposited after short range transport. Long range transport causes flake formation on obstacles and neutralisers, but little and deuterium rich (D/C $\approx$ 0.7) deposition in remote areas. The rest is leaving via the pumps in gaseous form. This behaviour is different from that in JET where large amounts of deuterium rich deposits were found in the louvers. Tungsten is favoured for the ITER divertors because of its low sputtering yield for hydrogen, but melting and erosion by carbon may be an additional concern. The short range transport of tungsten has been investigated in a well defined experiment and quantitatively re-constructed by means of the ERO-TEXTOR code. Code validation is necessary in order to increase the confidence and the applicability to JET and ITER.

Keywords: Plasma-wall interaction; Carbon transport balance; Tungsten erosion/deposition; Hydrogen retention; TEXTOR; ERO-TEXTOR code

1. Introduction

Appropriate selection of materials for the plasma facing components remains a crucial issue for future fusion devices aiming at long pulse operation as for example 400 s in ITER [1]. Not only the life time of the wall elements will be reduced due to erosion, but also accumulation takes place if the eroded material is transported to areas less affected by the plasma ions. Predictions are difficult to make, because present day machines need to integrate numerous plasma pulses in order to approach long term behaviour on the one hand. On the other hand, modelling of the transport processes requires experimental validation of the computer codes.

Most critical seems to be the divertor region. According to [1] the highest thermal (<10–20 MW/m^2) and particle (<10^{24} DT/m^2 s) loads are expected at the strike zone of the ITER divertor. Carbon fibre composites (CFC) are foreseen for these wall components ($\approx$50 m^2) because of the good form stability and the high sublimation temperature (3350 °C). However, carbon shows effective (percent range) chemical erosion by hydrogen [2], which diminishes the life time if the eroded material is not effectively re-deposited. Side walls, dome and private region ($\approx$140 m^2, $\approx$3 MW/m^2) of ITER are going to be protected by tungsten in order to benefit from the high melting temperature (T_m = 3407 °C) and the low sputtering yield (10^{-5}–10^{-4} for $T_e \approx 30$ eV). This will avoid intolerable high parasitic radiation of the released

* Corresponding author. Tel.: +49-2461 61 3203; fax: +49-2461 61 2660.

E-mail address: p.wienhold@fz.juelich.de (P. Wienhold).

0022-3115/03/$ - see front matter
PII: S0022-3115(02)01347-8

tungsten ions, but may become deteriorated [3] by additional erosion due to the carbon from the strike zones or by melting due to disruptions [1]. Part of the released tungsten will return to the surface by prompt re-deposition, but it is not yet clear which distances it can travel during long term operation.

In contrast to tungsten, carbon has a high probability for long range transport to remote areas where it can accumulate because of the reduced or absent hydrogen ion flux. Carbon mainly forms hydrocarbon radicals CH_x after the chemical erosion which can show low sticking probabilities (10^{-4} for CH_3 at 320 K [4]). The sticking can, however, increase by the formation of higher hydrocarbons [5] and lead to the deposition of hydrogen rich carbon layers. This will increase the radioactive tritium inventory in fusion devices. Observations made at JET [6] suggest that up to 1 kg of deuterium rich carbon ($D/C \approx 0.8$) had been accumulated within about 10^4 s at the water cooled louvers adjacent the inner divertor and partly flaked off during the Mark IIa operation phase. The material contained most of the tritium (≈3 g) remaining in the machine despite thorough cleaning procedures. The question is not answered yet how carbon accumulation and tritium co-deposition could be controlled, in particular in the non-accessible remote areas.

At TEXTOR, short range transport of carbon [7] and accumulation with rates up to 6–9 nm/s into regions behind obstacles with respect to the plasma flow (so called shadowed areas [8]) have already been investigated and partially modelled by means of the ERO-TEXTOR code [9]. It simulates chemical and physical erosion and the local transport and re-deposition of carbon and other impurities under tokamak plasma conditions. To improve the applicability of the code to JET and to ITER new experiments have been carried out at TEXTOR and dedicated to code validation. Two issues will be discussed in the following: (i) the quantification of the major carbon sources and the short and long range transport to the sinks after long term operation of TEXTOR. These observations will be compared to the findings in JET. (ii) The experimental observation of the local transport of tungsten into shadowed regions and the modelling by means of the ERO-TEXTOR code. Validation of the codes with well defined experiments is indispensable in order to model observations made in larger machines or to make predictions. This will be illustrated by two examples: the simulation of the carbon flux to the inner louver [10,11] of JET and the carbon gross erosion and re-deposition expected at the inner divertor plate of ITER.

2. Carbon transport and balance in TEXTOR

2.1. The major carbon source

In contrast to JET where vessel and strike zones at the divertors are the major carbon sources [12], the plasma–wall interaction in TEXTOR mainly takes place at the toroidal belt limiter. This limiter consists of eight blades

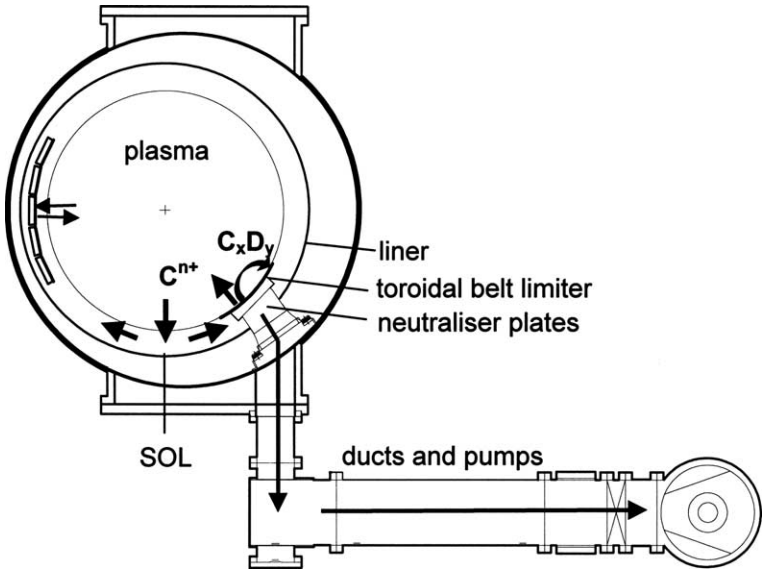

Fig. 1. Schematic of the poloidal cross-cut of TEXTOR to illustrate the locations of liner, toroidal belt limiter, neutraliser plates and pump ducts. The arrows indicate the major carbon sources and sinks as described in the text.

placed 45° below equatorial position (see schematic in Fig. 1) each covered with 28 graphite tiles (96×154 mm^2) which are mounted in two rows (2×14) on the blade. The surface area (3.4 m^2) covers about 10% of the total inner surface of the torus. Because of the non-circular poloidal curvature of the tiles only the central part of the blades limits the plasma at the small radius $r = 46$ cm while the outer regions rise into the scrape-off layer (SOL) by about 2 cm. This leads to a poloidal asymmetry of the incident field lines [13] and of the carbon erosion and deposition pattern. Part of the eroded carbon is directly deposited onto the surface of the tiles itself. The rest enters the plasma and is transported to obstacles (poloidal limiters, antennae protection limiters) in the SOL or enters the pump ducts behind the blades where it can stick on the neutraliser plates or is pumped out (Fig. 1). Other parts of the wall (liner [14], inner bumper limiter) seem to contribute little to the carbon exchange.

To measure the carbon net erosion at the toroidal limiter a new technique has been developed, the details of which are subject of another paper [15]. Only some information and results will be given here. One representative tile (no. 20, blade 5) had been polished before mounting and instrumented with drill holes (5 mm diameter, 0.15–0.45 mm deep) in nine toroidally oriented rows of three holes each (see Fig. 2). The bottoms of the holes were protected by tungsten (≈200 nm) which in contrast to the graphite surrounding is not eroded. They served as stable reference points for the surface profiles taken along the rows by means of a laser profiler before and after plasma exposure. The differences, i.e. the net erosion or deposition could be determined with an accuracy of about 1 μm. Some deposition found in the holes was identified by SIMS depth profiling and taken into account as off-set.

In the central part of the graphite tile the erosion was found to be ≈10 μm. This can be explained by the deuterium ion fluxes of $\approx 3 \times 10^{17}$ cm^{-2} s^{-1} as determined by the integration of the D_α light over the poloidal extension of the tile taking into account the total exposure time of 7625 s (March–August 2000) and provided that the erosion yield is 4%. In the area more distant from the plasma ($r \approx 47$ cm) the erosion is found to be larger (up to 28 μm) which is partly due to the enhanced flux of charge exchange neutrals in this region as has been calculated by the B2-EIRENE code (1.4×10^{17} cm^{-2} s^{-1} for an ohmic discharge). Towards the end of the tile ($r = 47.5$ cm) the erosion rate decreases again. In the average 11.3 μm were lost at 2/3 of the surface area which corresponds to 0.21 g of graphite (1.86 g/cm^3) for the single tile or to 46 g for the whole toroidal belt limiter. Related to the total plasma exposure time this value results into a carbon source strength of ≈22 g/h. The part of the surface (1/3) closest to the LCFS ($r < 46.5$ cm) cannot be reached by ions because of the almost grazing incidence (<0.5°) of the field lines. It turned to a net deposition zone.

2.2. Short range carbon transport

A large part of the eroded carbon is directly deposited on the tile's surface itself as can be seen in Fig. 2. It shows a view in the poloidal direction. The visible drill holes range from row 4 (top) in the erosion dominated

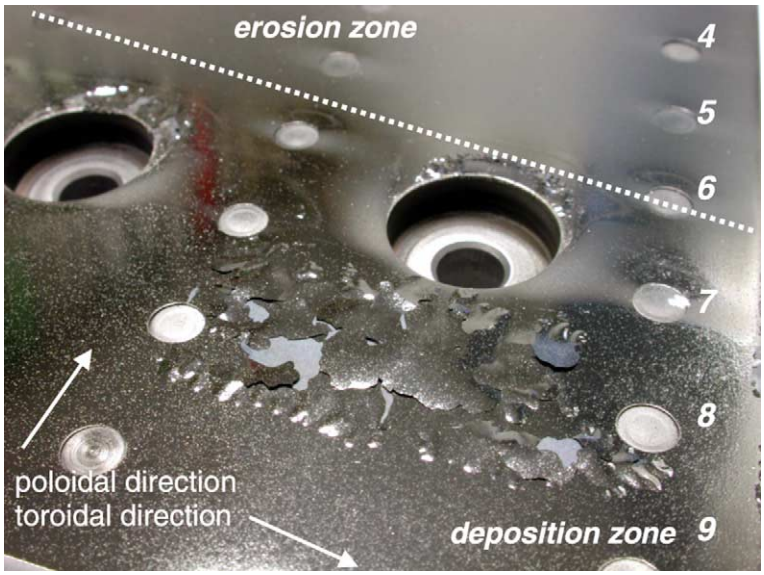

Fig. 2. View on limiter tile 20 (blade 5) after 7625 s of plasma exposure and dismounting. Flakes of 10 μm thickness in the deposition zone peel off after a mechanical shock. The drill holes in row 9 are closest to the LCFS.

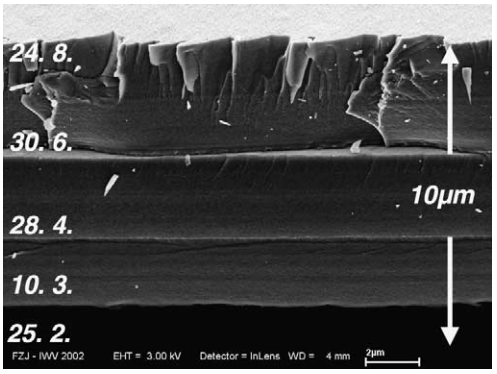

Fig. 3. SEM image of a flake grown in the deposition zone between 25.2.2000 and 24.8.2000 (7625 plasma seconds). The equidistant stratification corresponds to the three boronisations (100 nm of a-B:D) applied in equal time intervals and indicates the continuous growth.

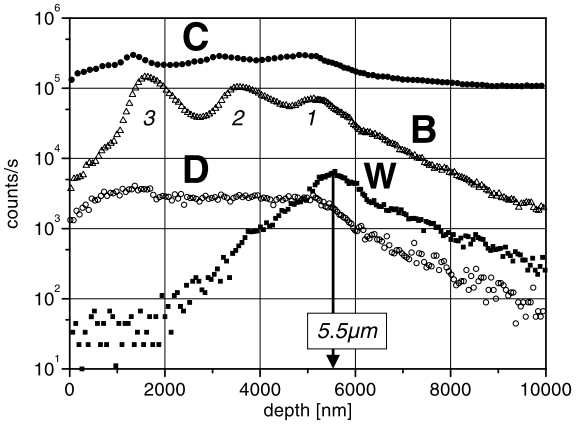

Fig. 4. SIMS depth profile in the erosion area, but in the center of a drill hole of row 3. The co-deposit (C, D) of 5.5 μm thickness ends at the W interlayer. Three maximums in the B signal are due to the three boronisations. The signals are not normalised.

zone up to row 9 (bottom) in the deposition zone which is the central part of the limiter blade ($r = 46$ cm). The third hole of each row is not visible in the figure. The two zones are separated by a dashed line passing the two bolt holes. While the erosion zone remained polished, the deposition zone became rather uniformly covered by a layer of ≈10 μm thickness as has been determined by SIMS depth profiling at several locations. This value is confirmed by SEM [16] of flakes peeled off the substrate after a mechanical shock (Fig. 3). Since we do not expect more than ≈5% [17] of impurities (mainly boron) in the films and 5–15% of deuterium [18] the value corresponds to 92 mg of carbon deposited on 1/3 of the surface, or to about 20.5 g if the 224 tiles of the belt limiter are considered. Related to the total exposure time this sink counts with ≈10 g/h. As Fig. 3 shows the deposited layer is stratified equidistantly according to the three boronisations applied in equal time intervals. It separates the strata by a thin (≈100 nm) boron marker. The net deposition rate remains nearly constant over an operation period of several month.

Obviously, part of the carbon – after erosion – has been transported over short distances only and is directly re-deposited. This is suggested by SIMS depth profiling in the centers of the drill holes after the exposure. One example taken at row 3 right in the erosion dominated zone is given in Fig. 4. The presence of a deuterium containing carbon film is indicated here by the co-deposited C and D. It ends at a depth of 5.5 μm where the W signal of the substrate occurs and the D signal drops simultaneously. Note, that the count rates do not reflect the relative concentrations of the species. It is rather unlikely that this film is formed by carbon drifting out of the SOL plasma because of the shallow [13] incident field lines (≈1°). The 0.3 mm deep and 5 mm wide hole remains shadowed for C^{4+} ions with typical Larmor radii of 1 mm. Ionic hydrocarbon radicals, however, eroded in the direct surrounding and redeposited on the bottom would remain there because the eroding D^+ ion flux is shadowed as well ($r_L \approx 1.6$ mm). This fact demonstrates the high sensitivity of the net effects on surface imperfections in areas of shallow incidence: grooves of few tenth of a mm can switch easily net erosion into net deposition even on plasma wetted components. Erosion in the shadowed grooves is then only due to neutral hydrogen [7].

Fig. 4 additionally shows three equidistant maximums of the boron signal according to the three boronisations. Obviously the layer has grown continuously during the exposure time while the environment became eroded. This behaviour has been investigated systematically for all the drill holes, and the results are summarised in Fig. 5. Independent on the poloidal location of the hole, the three maximums of the boron signals remain equidistant and indicate that the local carbon transport and the re-deposition processes are distributed over the extended surface. Only the rates of re-deposition into the holes increase from row 1 towards row 9 because of the shrinking distance to the LCFS. This likely leads to the decrease of the ionisation lengths of the released hydrocarbon radicals and to an according increase of the probability to return to the surface.

2.3. Long range carbon transport

Carbon not re-deposited directly enters the plasma and is transported as C^{n+} ions to other locations. Protruding obstacles as e.g. the poloidal limiters and the protection tiles for the ICRH antennas contribute remarkably as sinks [19]. Their effective area is small (≈0.2

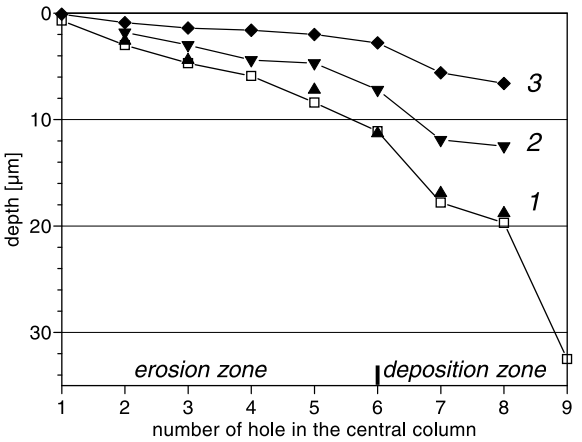

Fig. 5. Locations of the three maximums of the boron signals as taken from the SIMS depth profiles in the centers of the drill hole. The numbers refer to the three successive boronisations. The total thickness (open squares) of the deposits was determined from the disappearance of deuterium signal.

m^2), but the average net deposition rate is as high as ≈4–5 nm/s because of the perpendicular intersection of the field lines. Such values have often been observed by means of collector probes in the SOL of TEXTOR and result into a carbon accumulation rate of about 6 g/h. The co-deposition of hydrogen is low ($\approx 4 \times 10^{-4}$ [20]) due to the occasional temperature excursions of these components.

Other surfaces do not take part much to the carbon interchange. The contribution of the torus shaped and boronised liner ($r = 55$ cm) approaches zero [14]. It serves as a small but permanent source of boron instead. Little information is available at present for the graphite bumper limiter (≈6 m^2, $r = 49$ cm) on the high field side. SIMS depth profiles taken at several locations on a tile which was exposed together with the instrumented tile suggest a slight net deposition of no more than 0.5 μm over about 2/3 of the total area which results into a rate of 1–2 g/h of carbon. This contribution is lowered, however, by some carbon release from the other part of the surface which could not yet be determined.

The rest of the carbon (≈5 g/h) not found inside the torus should have left via the pump ducts. It is guided by the leading edges of the belt limiters together with the deuterium plasma ($\Gamma_{D^+} = 1$–5×10^{18} $cm^{-2}\,s^{-1}$ [21]) behind the blades. The carbon impurity flux leads to impressive net deposition on the neutraliser plates where it has grown up to thick crusts (mm) within five years of operation. Most of the material could be scratched off and the amount determined by weighing to 23.1 g [16]. The deuterium content does not exceed ≈0.5% because of the occasional temperature excursions of the loosely bound material during operation (surrounding temperature 350 °C). Taking into account the total plasma exposure time of ≈24 h the value stands for another 1 g/h. Obviously re-erosion takes place due to the deuterium ions of roughly 200 eV energy, but only little deposition was found on the inner areas of the cold pump ducts [14] where soft films ($n \approx 1.5$) are formed of thicknesses which could be estimated by interference fringe analysis. Although the contribution to the carbon balance (0.02 g/h) is negligible the films contain 100–1000 times more deuterium ($D/C \approx 0.7$) than the other deposits and their uncontrolled formation in fusion devices would increase the tritium content.

Most of the carbon released at the neutraliser plates seems to be neutral methane molecules and is pumped out. Observations made with a sniffer probe [21] suggest an erosion yield of 1% and, hence a rate of 1–2 g of carbon/h leaving the system in gaseous form. The remainder of 2–3 g/h still missing in the balance could not be identified.

2.4. Discussion

It is not a surprise that the balance of sources and sinks is not levelled out because of the uncertainties of the extrapolations. The value of this attempt could, however, be the better understanding of the processes. From the observed maximum carbon erosion rate of 13 μm/h one could figure out a 12 cm loss within a burn year or – assuming that a surface area of 10 m^2 is affected – about 2 tons of carbon lifted off and shifted either by short or by long range transport to other locations. For ITER, a prediction of absolute quantities is difficult to make, but the possible short range transport process of carbon could trigger unexpected re-deposition at surface imperfections or in shadowed areas near the strike zones and lead to the formation of tritium rich films.

The long range transport of carbon to the remote areas ends differently in JET and in TEXTOR. While in JET the majority of the carbon which enters the inner divertor seems to leave it towards the pumps and may become trapped as deuterium rich material ($D/C \approx 0.8$) at the water cooled structure of the louver, in TEXTOR great parts precipitate on the hot neutraliser plates ($D/C \approx 5 \times 10^{-3}$) or leave the system as saturated hydrocarbon. Only small fractions remain as deuterium rich films ($D/C \approx 0.7$) in the cool pump ducts. The most probable reason for this drastically different behaviour could be the different plasma temperatures and, hence ion energies in the JET divertor and at the TEXTOR neutralisers. At the hot neutralisers hard carbon films are formed because of the co-deposition with deuterium ions of several 100 eV ($T_e \approx 20$–50 eV). The re-eroded methane has little chance to stick. For JET, T_e ranges below 2–5 eV in the inner divertor which may enhance the formation of soft and polymer like films which are thermally unstable and show high chemical erosion. This

could lead to the formation of unsaturated hydrocarbon radicals C_xD_y with probably much higher sticking probability [5]. The possible influence of the substrate temperature is not fully clarified [22,23] yet.

The total amount of deuterium retained in TEXTOR due to co-deposition was estimated to be 5.6×10^{22} D/h by taking into account the different contents in the various sinks of carbon. This value is of the same order of magnitude as already found earlier [19]. It is about 10% of the fuel rate (5.5×10^{23} D/h) introduced via the gas inlet system during plasma pulses as extracted for the operation period March–August 2000. Contributions by neutral beam heating (mostly H in TEXTOR) are neglected in a first approximation. Similar high retention has been reported from JET [24] and illustrates the concern about the radioactive tritium inventory to be expected if carbon is used. Note, that the greatest part of D is retained on the plasma wetted surfaces of the toroidal limiter in TEXTOR while in JET mainly the remote areas are affected.

If tritium rich carbon could not be removed from the remote areas of ITER the safety limit (350 g) will be achieved rather soon. Probably the formation and the re-erosion of hydrogen rich deposits can be influenced by making use of their dependence on ion impact energies and on substrate temperature. But, the way to securely control tritium is not developed yet. Further investigations are needed and the predictions for larger machines have to be based on computer codes. Codes, however, must be validated by means of special experiments which can be carried out also at smaller machines like TEXTOR.

3. Local transport of tungsten and silicon and its modelling

3.1. Experimental

Although low sputtering yields (10^{-4}) for hydrogen on tungsten are expected in ITER the erosion might increase (10^{-1}) due to the presence of carbon ions. Tungsten may also melt by thermal impact. Part of the tungsten not promptly re-deposited will locally be transported, but it is not clear yet which distance it could travel. A special experiment has been set up in TEXTOR where the local transport of tungsten and of silicon (for comparison) and their accumulation in a shadowed region were investigated and the results quantitatively modelled by the ERO-TEXTOR code. Since a similar experiment for carbon accumulation has already been described elsewhere [8] only a short description will be given.

A graphite block (see Fig. 6) with an inclined surface (20°) was positioned in the SOL 1 cm outside the LCFS. It was covered with a polished graphite plate which carried an interlayer of Re (≈140 nm) and of W (≈100 nm), but protected on top by a thin transparent silicon film (≈150 nm of a-Si:D). A small strip of 12 mm (still visible) had been carbonised instead (≈300 nm of

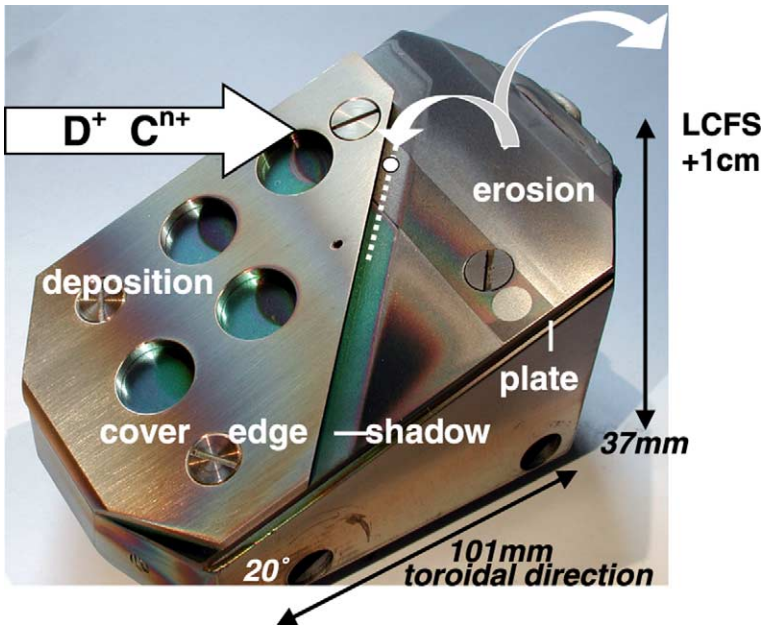

Fig. 6. Photograph of the graphite target after 150 s of plasma exposure and dismounting. The Si–W–Re film (390 nm) is totally eroded at the plasma near edge (LCFS + 1 cm) and the elements have partly been transported into the shadowed region where SIMS depth profiling was carried out along the dotted line.

a-C:H). This plate was partly covered by an aluminium lid (3 mm) having a sharp edge which created a local shadow region (8.3 mm wide) with respect to the ions following the field lines. Note, that the shadow crosses the target plate diagonally and that the radial distance to the LCFS shrinks towards the upper end (LCFS + 1 cm). Holes in the protection plate allowed to investigate deposition in front of obstacles (not subject of this paper).

The arrangement was exposed to 26 ohmic discharges ($n_{eo} = 2.75 \times 10^{19}$ m^{-3}, $I_p = 350$ kA, $B_T = 2.25$ T) corresponding to 150 plasma seconds. Electron densities and temperatures in the plasma edge were measured by means of He- and Li-beam diagnostics resulting into an ion flux of $\Gamma_{D^+} = 1.7 \times 10^{19}$ cm^{-2} s^{-1} at the LCFS with a decay length of about 8 mm. During exposure the surface was inspected by colorimetry and the released particles observed by spectroscopy, after exposure it has been investigated by colorimetry and by ion beam analyses for depth profiling (SIMS, AES) and for the concentrations (NRA, RBS, EPMA). Fig. 6 shows the appearance of the sample after dismounting. Obviously, the metal film (Si, W, Re) has totally been eroded in an ≈18 mm wide zone near the LCFS. Part of this material is accumulated in the shadowed region and is visible as shiny layer on the carbonised strip. The other parts of the shadowed region still showed the initial green interference colour of the a-Si:D film which means that the thickness change is less than few nm. Net deposition starts beyond ≈2.2 cm off the LCFS on the plasma far part of the sample. The deposit became visible as a coloured film on the aluminium plate. The maximum net deposition rate on the inclined target was found to be +0.8 nm/s.

3.2. Results

Fig. 7(a) shows the normalised depth profiles taken by SIMS in the carbonised zone in the shadow (dot in Fig. 6). Note, that the logarithmic abscissa expands the surface near distances and compresses the bulk. Re, W, and Si appear at the very surface (until ≈30 nm) and can be discriminated on top of the still present a-C:H film (≈300 nm). Below the carbon the two interlayers W and Re show up as sharp peaks which separate the carbon film from the graphite bulk (≈450 nm). It is obvious that the initial sequence Si, W, Re has exactly been reversed. The species have been eroded and transported into the shadowed region one after the other. The successive erosion during exposure was observed by the appearance and disappearance of the Si II and the W I light intensity. Camera inspection of the erosion zone between plasma pulses revealed the gradual shrinking of the coated area and the arrival of the metals in the shadow. The total erosion was completed within ≈100 s which corresponds to an average net erosion rate of −4 nm/s.

Fig. 7(b) shows depth profiles for tungsten only, but taken in the shadow along the dotted line in Fig. 6. The

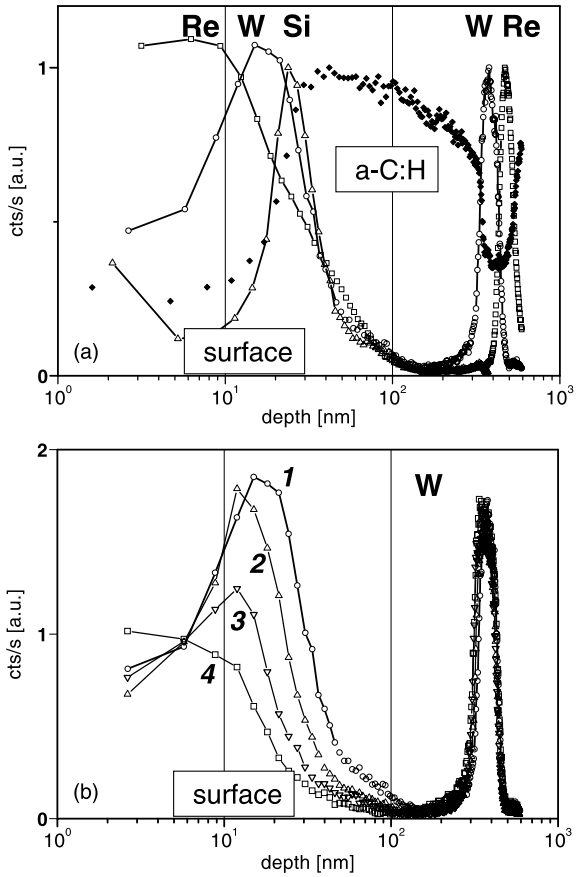

Fig. 7. SIMS depth profiles in the shadowed region (a) of Re, W, Si and C at a single spot and (b) of W at locations with increasing distances from the erosion zone. The numbers 1, 2, 3, 4 correspond to 14, 17, 20, 22 mm distance, respectively. Note, that the logarithmic expanded abscissa pronounces the surface compared to the bulk.

surface concentration decreases with increasing distance from the location of the source. Such behaviour is expected if part of material returns to the surface after erosion and local transport. The surface concentrations drop to one half within 1 cm while the bulk's remain unaffected. Re behaves identically, but Si shows a steeper decay. The erosion and the local transport of the metallic species across the surface were subject of the quantitative modelling by means of the ERO-TEXTOR code and described in the following.

3.3. Simulations with the ERO-TEXTOR code

The amounts of tungsten and silicon deposited on the surface in the shadowed region were determined by taking into account the peak areas and the different widths of source (18 mm) and sink (8.3 mm). The amount of e.g. tungsten ranges between 3% and 8% of

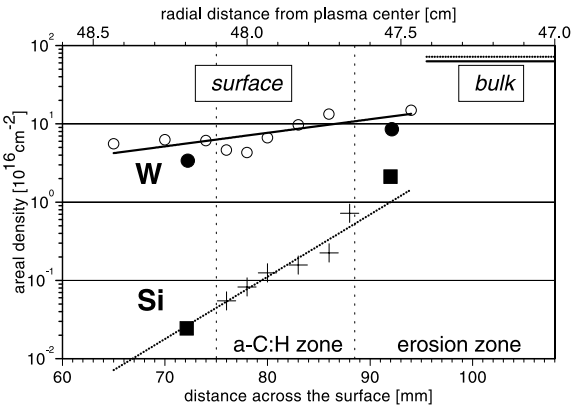

Fig. 8. Areal concentrations for W and Si as determined for the bulk by RBS and EPMA and for the surface as determined from the peak ratio of the SIMS profiles in dependence on the distance to the erosion zone. The ERO-TEXTOR code simulation yield agreement if $D_\perp = 0.2$ m^2/s for W (dots) and $D_\perp = 0.02$ m^2/s for Si (squares) are used.

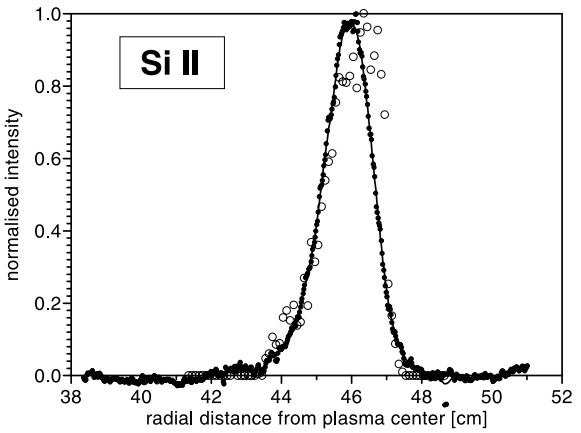

Fig. 9. Si II light intensity observed (dots) in poloidal direction above the inclined target and calculated (open circles) by means of the ERO-TEXTOR code.

the eroded amount. For Si up to 0.4% were found only. The values have been calibrated by help of the areal densities as determined by the ion beam analyses. The results are given in Fig. 8. The initial bulk concentrations of 6.3×10^{17} cm^{-2} for W and 7.2×10^{17} cm^{-2} for Si corresponding to 100 nm and 150 nm, respectively (bars) were completely eroded. The amounts arriving at the surface in the shadow are given as circles (W) and crosses (Si) and decrease according to Fig. 7(b).

The simulation calculations aimed at the quantitative re-construction of the findings at two 2 cm distant locations close ($x = 92$ mm) and far ($x = 72$ mm) to the source. The Monte-Carlo code ERO-TEXTOR does not only take into account the plasma parameters ($T_e = 70$ eV, $n_{eo} = 2.5 \times 10^{18}$ m^{-3} at the LCFS) and a carbon impurity flux (2% of Γ_{D^+}) [1], but also the sputtering yields, ionisation lengths, $E \times B$ forces and friction. Since little is known about the cross-field diffusion constants, a value of 0.2 m^2 s^{-1} (as for carbon) was used for tungsten. The calculated amounts for deposition coincide well (full dots) with the experimental results. For silicon which shows very low deposition efficiency [25] an accordingly lower diffusion constant (0.02 m^2 s^{-1}) fits the data (full squares).

Two transport mechanisms were distinguished which contribute differently: while for tungsten repetitive prompt deposition (≈50%) within the first Larmor orbit [26] seems to play a big role, the silicon transport is dominated (≈70%) by re-deposition after the ionisation of the eroded Si in the SOL plasma. Accordingly, the observed Si II emission appeared further distant (≈10 mm) from the probe's head than the W I light (≈5 mm). The larger ionisation length for Si explains the lower re-deposition efficiency compared to W. The values were used to cross-check the calculations with the spectroscopic observations. Fig. 9 shows as example the agreement between the measured and the calculated radial profiles of the Si II light emission.

3.4. Discussion

It is unlikely that the erosion rate of −4 nm/s observed on the inclined target is only due to the deuterium ion flux ($\Gamma_{D^+} = 7 \times 10^{18}$ cm^{-2} s^{-1} at $r = 47$ cm). This flux could erode the a-Si:D layer and only part of tungsten (sputtering yield 1.7×10^{-3} [27]) during the time of exposure, but not the whole layer. Obviously carbon ions (1–2% of Γ_{D^+}) have eroded effectively the metallic species because of there high yield of ≈0.18. In ITER, the electron temperature is lower (>30 eV at the baffles) than in the experiment (60 eV), but erosion by carbon could become serious because the sputtering yield remains still high enough (≈0.12). In particular if long pulse operation is aimed at possible erosion by carbon from the strike zones should be considered. However, the net erosion rate of tungsten is difficult to estimate, because the carbon can also form films on the surface [28]. But an erosion rate of −4 nm/s for tungsten would correspond to 1.6 mm within 1000 pulses or to 13 cm per burn year. Whether the tungsten will locally be transported to other areas with 1–2 cm/100 s (40 m/1000 pulses) as observed in the experiment has to be shown in simulation calculations. Tungsten accumulated in shadowed regions could cause the formation of flakes. The observed accumulation rate of 0.1–0.3 nm/s would correspond to 80 μm/1000 pulses.

[1] The value of 1–2% could be determined independently due the discrimination of the D^+ and C^{n+} fluxes at the sharp edge of the Al cover.

Although the erosion experiments described here do not allow direct extrapolations to ITER they can yield relevant data in order to validate computer codes which model and simulate the processes. The fact that the ERO-TEXTOR code could re-construct quantitatively the experimental findings is a strong argument for its application to JET and ITER.

4. Outlook

It has to be shown that the wall materials foreseen for ITER (CFC and tungsten in the divertor region and beryllium for the main chamber walls) are an optimum for the long pulse operation. Unavoidable related to the use of carbon is the question how the tritium retention can be controlled. A carbon erosion/deposition balance as established for TEXTOR or special experiments to investigate local tungsten transport or other experiments in smaller machines are difficult to scale up to ITER dimensions. But they become relevant if the observations can be modelled by computer codes which allow the extrapolation. The improvement of such codes and their continuous validation on experiments seems to be the major conclusion we have to draw. The quantitative simulations of the results by means of the ERO-TEXTOR code is therefore one important step.

Consequently, this code has been applied to simulate the observed local carbon transport in JET. As mentioned above the asymmetric carbon flow from the outer to the inner divertor leads eventually to massive and deuterium rich carbon deposition at the inner louvers. A flux ratio $\Phi_C/\Phi_D \approx 4\%$ to the louvers has been estimated [6], but carbon is also deposited near the strike zones. Since the attempts to simulate this behaviour by means of the ERO-TEXTOR code are outlined in [10] they will not be discussed here. But the modelling suggests a carbon re-deposition near the strike zones in the form of 'soft' films. The films show enhanced re-erosion likely in the form of higher hydrocarbons which are transported step wise across the surface in the direction to the louvers. Here they accumulate because of the absence of plasma and if a high sticking probability can be assumed.

First attempts to apply the code to ITER were made in order to estimate carbon gross erosion and re-deposition on the vertical divertor plates [29]. Fig. 10 shows as example that for the reference case (410 MW fusion power at $Q = 10$) the gross erosion at the inner strike zone ($T_e = 1 - 2$ eV, $n_e = 1 - 2 \times 10^{21}$ m^{-3}) exceeds 40 nm/s. Only 83–94% (depending on sticking probability) will be re-deposited, but not at the same location. The lifted off and re-deposited carbon would give rise to co-deposition of roughly half a gram of tritium at the affected area ($\approx$2.5 m^2) within one pulse and the safety limit will be achieved in less than 700 pulses. Net erosion will cause grooves in the CFC of 5–10 mm depth within a 1000 pulses if the impurity fluxes (mainly beryllium) out of the main chamber are not considered. Erosion turns e.g. to deposition if the fraction of beryllium is 0.5%, but the intermixing of the materials makes further predictions very complex.

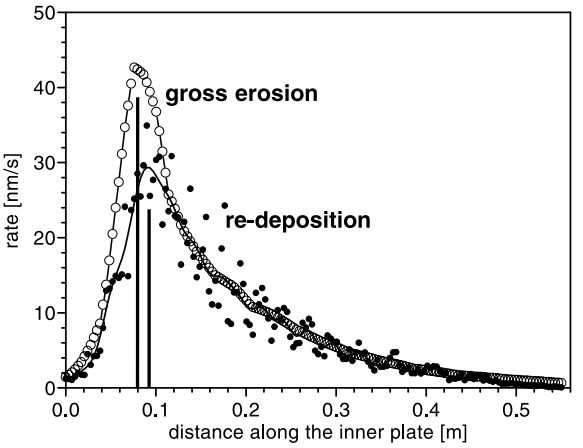

Fig. 10. Gross erosion of CFC (circles) and carbon re-deposition as calculated by the ERO-TEXTOR code for the inner divertor plate of ITER. Impurity fluxes out of the main chamber are omitted.

The results depend strongly on the input parameters which have to be either assumed or delivered from other codes. Coupling to other codes which can treat the global transport or the material mixing is therefore inevitable.

Acknowledgements

The technical assistance of M. Freisinger and H. Reimer, and the B2-EIRENE code calculations made by P. Börner and D. Reiser have greatly been acknowledged.

References

[1] G. Federici, C.H. Skinner, J.N. Brooks, J.P. Coad, C. Grisolia, A.A. Haasz, A. Hassanein, V. Philipps, C.S. Pitcher, J. Roth, W.R. Wampler, D.G. Whyte, Nucl. Fusion 41 (12R) (2001) 1967.
[2] J. Roth, E. Vietzke, A.A. Haasz, Suppl. Nucl. Fusion 1 (1991) 63.
[3] K. Krieger, H. Maier, R. Neu, ASDEX Upgrade Team, J. Nucl. Mater. 266–269 (1999) 207.
[4] C. Hopf, T. Schwarz-Selinger, W. Jacob, A. von Keudell, J. Appl. Phys. 87 (2000) 2719.
[5] M. Maier, A. von Keudell, J. Appl. Phys. 90 (2000) 3585.

[6] J.P. Coad, N. Bekris, J.D. Elder, S.K. Erents, D.E. Hole, K.D. Lawson, G.F. Matthews, R.-D. Penzhorn, P.C. Stangeby, J. Nucl. Mater. 290–293 (2001) 224.
[7] P. Wienhold, H.G. Esser, D. Hildebrandt, A. Kirschner, M. Mayer, V. Philipps, M. Rubel, J. Nucl. Mater. 290–293 (2001) 362.
[8] P. Wienhold, M. Rubel, M. Mayer, D. Hildebrandt, W. Schneider, A. Kirschner, Phys. Scr. T94 (2001) 141.
[9] A. Kirschner, V. Philipps, J. Winter, U. Kögler, Nucl. Fusion 40 (5) (2000) 989.
[10] A. Kirschner, J.N. Brooks, V. Philipps, J.P. Coad, Plasma Phys. Control. Fusion, submitted for publication.
[11] J.N. Brooks et al., these Proceedings. PII: S0022-3115(02)01405-8.
[12] M. Mayer, R. Behrisch, K. Plamann, P. Andrew, J.P. Coad, J. Nucl. Mater. 266–269 (1999) 604.
[13] T. Denner, thesis D61, Univ. Düsseldorf, Germany, Jül-3610, 1998.
[14] J. von Seggern, P. Wienhold, T. Hirai, V. Philipps, these Proceedings. PII: S0022-3115(02)01411-3.
[15] M. Mayer, P. Wienhold, D. Hildebrandt, W. Schneider, these Proceedings. PII: S0022-3115(02)01357-0.
[16] M. Rubel, V. Philipps, P. Wienhold, M. Freisinger, W. Jacob, J. Linke, J. von Seggern, E. Wessel, 11th International Workshop on Hydrogen Isotope Recycling at Plasma Facing Materials in Fusion Reactors, University of Tokyo, Japan, 22–24 May, 2002; Phys. Scr., in press.
[17] P. Wienhold, H.G. Esser, D. Hildebrandt, A. Kirschner, K. Ohya, V. Philipps, M. Rubel, J. von Seggern, Phys. Scr. T81 (1999) 19.
[18] M. Rubel, P. Wienhold, D. Hildebrandt, J. Nucl. Mater. 290–293 (2001) 473.
[19] M. Mayer, V. Philipps, P. Wienhold, H.G. Esser, J. von Seggern, M. Rubel, J. Nucl. Mater. 290–293 (2001) 381.
[20] J. von Seggern, M. Rubel, P. Karduck, V. Philipps, H.G. Esser, P. Wienhold, Phys. Scr. T81 (1999) 31.
[21] V. Philipps, A. Pospieszczyk, H.G. Esser, et al., J. Nucl. Mater. 241–243 (1997) 105.
[22] V. Philipps, M. Stamp, A. Pospieszczyk, A. Huber, A. Kirschner, E. Vietzke, these Proceedings. PII: S0022-3115(02)01344-2.
[23] I.I. Arkhipov, G. Federici, A.E. Gorodetsky, C. Ibbott, et al., J. Nucl. Mater. 290–293 (2001) 394.
[24] P. Andrew, D. Brennan, J.P. Coad, J. Ehrenberg, et al., J. Nucl. Mater. 266–269 (1999) 153.
[25] H.G. Esser, J. Winter, V. Philipps, et al., J. Nucl. Mater. 220–222 (1995) 457.
[26] D. Naujoks, K. Asmussen, M. Bessenroth-Weberpals, S. Deschka, et al., Nucl. Fusion 36 (6) (1996) 671.
[27] U. Kögler, J. Winter, Jül-3361, March 1997.
[28] W. Eckstein, K. Krieger, J. Roth, J. Nucl. Mater. 258–263 (1998) 912.
[29] A. Kirschner, private communication.